A NUMERICAL STUDY ON CONDENSATION HEAT TRANSFER AND PRESSURE DROP CHARACTERISTICS OF LOW PRESSURE VAPOR IN A PLATE HEAT EXCHANGER

by

Zhongbin ZHANG*, Tianyu ZHANG, and Hao ZHANG

School of Energy and Power Engineering, Northeast Electric Power University, Jilin, Jilin Province, China

Original scientific paper
https://doi.org/10.2298/TSCI190914095Z

In this work, the condensation heat transfer and pressure drop characteristics of plate heat exchangers were simulated, and the 3-D temperature, pressure, and velocity fields were obtained. From the flow field, we can see that the velocity of vapor is higher than that of condensate. From the pressure field, we can see that the pressure shows a downward trend along the flow direction, and there is, the more pressure drop in the first half of the plate. From the temperature field, we can see that the temperature gradient increases with the increase of velocity and pressure gradient. Meanwhile, the effect of vapor mass-flow, dryness and superheat on condensation heat transfer coefficients and pressure drops were investigated. The results show that the pressure drop and heat transfer coefficient both increase with the increase of dryness, degree of superheat and mass-flow. In addition, the correlation equations developed to predict the condensation heat transfer and friction factor perfectly agree with the experimental results.

Key words: *condensation heat transfer, pressure drop, plate heat exchangers, correlation, numerical simulation*

Introduction

Plate heat exchangers (PHE) have gained increasing applications due to its advantages such as high heat exchange efficiency, small temperature difference at the end, compact and lightweight structure, strong interchangeability and convenient maintenance [1-5].

In addition, PHE are promising candidates for condensation processes since their geometries tend to break up the condensate and enhance the heat transfer. Thus PHE started to play an important role in the industrial operations used as condensers. A large amount of investigations concerning condensation in PHE has been extensively conducted in recent years. Furthermore, the attention almost is focused on refrigeration industry [6-10]. Several experiments have been carried out on condensation, resulting in heat transfer and frictional pressure drop correlations. Wang *et al.* [11] obtained the heat transfer and pressure drop characteristics of complete steam condensation and partial condensation. Han *et al.* [12] obtained the 3-D temperature, pressure and velocity fields using numerical simulation methods. Shi *et al.* [13] investigated the condensation of R134a inside a plate exchanger varying both vapor quality and mass flux.

* Corresponding author, e-mail: 290153610@qq.com

The first theoretical study undertaken on laminar condensation over cooled metal surfaces was the pioneering work of Nusselt, in which a correlation was developed [14]. The correlation was further developed by including the effect of heat capacity [15]. Jokar *et al.* [16] measured HTC during HFC-134a condensation inside BPHE and applied dimensional analysis to develop new heat transfer and pressure drop correlations. Kuo *et al.* [17] reported experimental data on HFC-410A condensation inside a BPHE and proposed empirical correlations for heat transfer and pressure drop.

Although numerous investigations have been carried out for condensation heat transfer, there are still some gaps in understanding the condensation process in PHE. Most of the former numerical studies relating to the condensing flow in mainly focused on the mini-channels. However, condensation in PHE is a very complicated process, involve various parameters such as quality, fluid property, mass flux, and local flow regimes. There is no information in the literature about Marangoni condensation in a PHE. Furthermore, the condensation mode in a PHE has not to be recorded in literature. Our investigation tried to carry out condensation experiments which different concentration ethanol-water mixtures was led into a PHE under different pressures. The present work mainly focuses on the effects of vapor mass-flow, dryness and superheat on heat transfer and pressure drop characteristics inside channel of herringbone PHE. Both of the heat transfer and pressure drop characteristics are important for a better understanding the condensation process and the design of more efficient heat exchangers or other heat dissipating equipment. In addition, we attempted to propose a new general correlation of the condensation heat transfer a, which can be broadly applied to the PHE.

Model development

Volume of fluid model

The volume of fluid (VOF) model [18] can solve momentum equations and track the liquid-vapor inter-facial volume fraction in the whole computational domain in order to simulate two immiscible fluids. All control volumes must be full of a single fluid phase or several fluid phases. In each cell, the volume fractions of all fluids sum to unity:

$$\alpha_l + \alpha_\mathrm{v} = 1 \tag{1}$$

where α is the volume fraction, l – the liquid phase, and v – the vapor phase.

The VOF model represents the fields for all variables and properties with volume-averaged values. Thus, the variables and properties of each control volume are depended upon the volume fraction values of each phase. The density, viscosity and thermal conductivity of each cell are calculated:

$$\rho = \alpha_l \rho_l + \alpha_\mathrm{v} \rho_\mathrm{v} \tag{2}$$

$$\mu = \alpha_l \mu_l + \alpha_\mathrm{v} \mu_\mathrm{v} \tag{3}$$

$$\lambda = \alpha_l \lambda_l + \alpha_\mathrm{v} \lambda_\mathrm{v} \tag{4}$$

where ρ is the density, μ – the viscosity, and λ – the thermal conductivity.

The liquid-vapor interface in VOF model is obtained by solving the volume fraction continuity equation of the second phase in the calculation unit. In this paper, the vapor phase

and the liquid phase are set as the first phase and the second phase respectively. The volume fraction equation is:

$$\frac{\partial \alpha_i}{\partial t} + \vec{\mathrm{v}}\nabla\alpha_i = \frac{m_i}{\rho_i} \tag{5}$$

The governing equations including the continuity equation, momentum equation, and energy equation are listed as follows.

– continuity equation

$$\frac{\partial \rho}{\partial t} + \nabla(\rho\vec{\mathrm{v}}) = 0 \tag{6}$$

where ρ is the density, t – the time, $\vec{\mathrm{v}}$ – the velocity.

– momentum equation

$$\frac{\partial}{\partial t}(\rho\vec{\mathrm{v}}) + \nabla(\rho\vec{\mathrm{v}}\vec{\mathrm{v}}) = -\nabla p + \nabla[\mu(\nabla\vec{\mathrm{v}} + \nabla\vec{\mathrm{v}}^T)] + \rho\vec{\mathrm{g}} + \vec{\mathrm{F}} \tag{7}$$

where p and μ are pressured in the flow field, $\vec{\mathrm{g}}$ – the acceleration due to gravity, $\vec{\mathrm{F}}$ – the body force acting on the system and viscosity of the flow system, respectively.

To take into account the effects of surface tension, the continuum surface force model proposed by Brackbill *et al.* [19] was adopted. Then the force at the surface can be expressed as a volume force and appeared as an additional source term in the momentum equation. The volume force $\vec{\mathrm{F}}$ was computed:

$$\vec{\mathrm{F}} = 2\sigma\frac{\rho\kappa_l\nabla\alpha_l}{\rho_{\mathrm{v}} + \rho_l} \tag{8}$$

where σ is the interfacial tension force between liquid and vapor. The gradient of the volume fraction scalar is adopted to calculate the interface curvature, κ.

$$\kappa = \nabla\frac{\nabla\alpha_l}{|\nabla\alpha_l|} \tag{9}$$

Energy equation:

$$\frac{\partial}{\partial t}(\rho E) + \nabla[\vec{\mathrm{v}}(\rho E + P)] = \nabla[\lambda(\nabla T)] + S_{\mathrm{h}} \tag{10}$$

where E, T, λ, and S_{h} are energy, temperature, effective thermal conductivity and heat source, respectively.

$$E = \frac{\sum_1^2 \alpha_{\mathrm{v}}\rho_{\mathrm{v}}E_{\mathrm{v}}}{\sum_1^2 \alpha_{\mathrm{v}}\rho_{\mathrm{v}}} \tag{11}$$

Turbulence model

The standard k-ε model for each phase was chosen to model the turbulence in the steam-water system. The standard k-ε model is a model based on model transport equations for the turbulence kinetic energy, k, and its dissipation rate, ε, and the equation is:

$$\frac{\partial}{\partial t}(\rho k)+\frac{\partial}{\partial x_i}(\rho k u_i)=\frac{\partial}{\partial x_j}\left[\alpha_k\left(\mu+\frac{\mu_t}{\sigma_k}\right)\frac{\partial k}{\partial x_j}\right]+G_k+G_b+\rho\varepsilon-Y_M+S_k \tag{12}$$

$$\frac{\partial}{\partial t}(\rho\varepsilon)+\frac{\partial}{\partial x_i}(\rho\varepsilon u_i)=\frac{\partial}{\partial x_j}\left[\alpha_\varepsilon\left(\mu+\frac{\mu_t}{\sigma_\varepsilon}\right)\frac{\partial\varepsilon}{\partial x_j}\right]+C_{1\varepsilon}\frac{\varepsilon}{k}\left(G_k+C_{3\varepsilon}C_b\right)-C_{2\varepsilon}\rho\frac{\varepsilon^2}{k}+S_\varepsilon \tag{13}$$

where μ_t eddy viscosity, G_k and G_b are the generation of turbulence kinetic energy due to the mean velocity gradients and buoyancy, respectively, Y_M is the contribution of the fluctuating dilatation in compressible turbulence to the overall dissipation rate. The constant are taken as $C_\mu = 0.09$, $\sigma_k = 1$, $\sigma_\varepsilon = 1.3$, $C_{1\varepsilon} = 1.44$, $C_{2\varepsilon} = 1.92$.

Phase-change model

The main difficulty encountered in condensation process is how to determine the relevant source term. In this paper, Lee [20] phase transition model evolved on the basis of Hertz Knudsen equation is used. It was assumed that the mass transfer process accompanied by the release or absorption of latent heat occurred at a constant pressure and the interface temperature was equal to T_{sat}. The following equations were added to the governing equations as a source term through the user defined functions. The liquid-vapor mass heat transfer can be described:

$$m_{\text{v}} = -m_l = \frac{r\rho_{\text{v}}\alpha_{\text{v}}(T-T_{\text{sat}})}{T_{\text{sat}}}, \quad T \le T_{\text{sat}} \tag{14}$$

$$m_l = -m_{\text{v}} = \frac{r\rho_l\alpha_l(T-T_{\text{sat}})}{T_{\text{sat}}}, \quad T > T_{\text{sat}} \tag{15}$$

where r is the phase transition coefficient. The value of phase transition coefficients were studied through the method of experiments and numerical simulations. It was found that the range of phase transition coefficients is very large from 0.001 to 10000. In this paper, after several simulation studies, the value of phase transition coefficient was determined to be 0.6.

Calculation method

In this study, simulations of the condensation heat transfer of low pressure vapor in channel of herringbone PHE is carried out using commercial CFD software ANSYS FLUENT. According to the actual size of BR0.015F herringbone plate, a 3-D physical model has been developed using commercial software. The calculation area is shown in fig. 1. The characteristic parameters are shown in tab. 1.

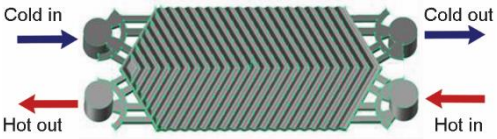

Figure 1. Geometric model of PHE

Due to the complex structure of PHE, the model is simplified and divided into 10 parts, and each part is filled with unstructured mesh, as shown in fig. 2. To verify the accuracy and validity of the numerical model, the results of Nusselt number have been compared. As shown in fig. 3, when the mesh step is 0.5 mm, the Nusselt number becomes stable. Considering the accuracy and efficiency requirements, the 1.44 million cells are adequate to obtain grid-independent results.

Table 1. Characteristic parameters of BR0.015F corrugated sheet

Characteristic parameter	Value	Characteristic parameter	Value
Sheet size [mm]	258×100	Corrugated normal pitch [mm]	6
Corrugated angle [°]	120	Sheet thickness [mm]	0.6
Corrugated depth [m]	2	Heat transfer area [m^2]	0.015
Cornerpore diameter [mm]	20	Equivalent diameter [mm]	4
Distance between plates [mm]	2	Passageway sectional area [m^2]	0.000166

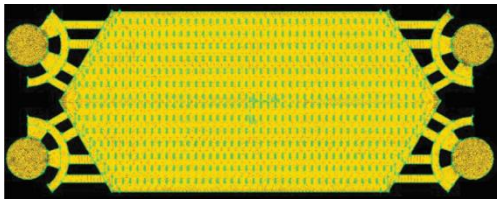

Figure 2. Model grid of PHE

In order to enhance the convergence of numerical calculation, velocity inlet boundary conditions is adopted for both steam and coolant inlets and pressure outlet boundary conditions is adopted for both steam and coolant outlets. The boundary condition of non-slip velocity is adopted on the wall of PHE. The wall between steam and coolant is the heat transfer surface, and other surfaces are considered to be adiabatic and have no heat loss. In this paper, user-defined function is used in FLUENT to define the quality source term and energy source term of condensation process, which is loaded into the control equation. The vapor phase and the liquid phase are set as the initial phase and the second phase respectively.

Results and analysis

Model validation and data reduction

To verify the accuracy and validity of the numerical model, the results have been compared with analytical solutions of two-phase flow with phase transition obtained by Alexiades and Salomon [21]. It is seen in fig. 4 that acceptable agreement has been obtained between numerical and analytical solutions.

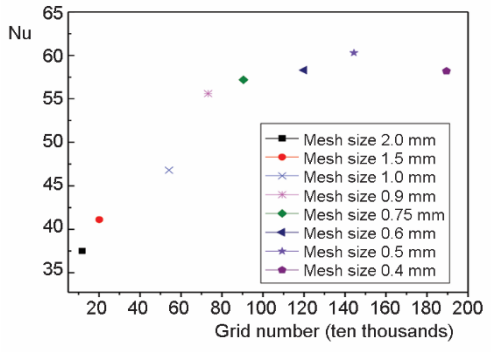

Figure 3. Grid independence verification

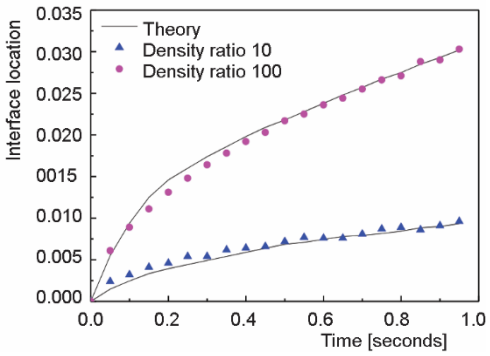

Figure 4. The position of phase interface varies with time

The primary data were fluid-flow rates, pressure and temperature at inlet and exit of the PHE for both fluids. The friction coefficient is defined:

$$f = \frac{\Delta p \frac{D_\mathrm{h}}{L}}{2\rho u^2} \tag{16}$$

where D_h is the hydraulic diameter, which was defined:

$$D_\mathrm{h} = \frac{4A_\mathrm{C}}{P} \tag{17}$$

The vapor-side heat transfer coefficient was then determined from:

$$\frac{1}{h} = \frac{1}{U} - \frac{1}{h_l} - R_\mathrm{wall} \tag{18}$$

In this equation the water-side heat transfer coefficient, h_l, was determined from a correlation previously developed from single-phase water-water PHE and U is the overall heat transfer coefficient, which is determined:

$$U = \frac{Q}{A\Delta T_\mathrm{LMTD}} \tag{19}$$

where A is the effective heat transfer surface area, ΔT_LMTD – the log-mean temperature difference, and Q – the heat transfer rate, which can be determined by energy balance:

$$Q = \dot{m}_l c_\mathrm{p} \Delta T_l \tag{20}$$

where ΔT_l is the difference in fluid temperature of liquid side between inlet and outlet conditions.

The Nusselt number is:

$$\mathrm{Nu} = \frac{hD_\mathrm{h}}{\lambda} \tag{21}$$

Velocity distribution characteristics

Figure 5 depicts the velocity contours of vapor and condensate on the y = 2 mm section in a PHE. By comparing figs. 5(a)-5(d), it can be seen that the velocity of vapor is higher than that of condensate. Since the condensate in the flow channel is initially attached to the plate, velocity of condensate is impacted by the gravity and shear force between the vapor and liquid. Therefore, the velocity of condensate is low.

In addition, along the direction of flow, the velocity of vapor-liquid two-phase flow increases continuously under the action of gravity, and the velocity difference between vapor and liquid is getting smaller and smaller. Comparing fig. 5(b) with fig. 5(d), it can be seen that the process of condensation is delayed in the inlet section due to the existence of superheat, and more heat transfer area is needed to vapor below the saturation temperature.

Pressure distribution characteristics

Figure 6 depicts the pressure contours of vapor side in a PHE with y = 2 mm cross-section. From the four graphs, we can see that the pressure shows a downward trend along the flow direction, and there is the more pressure drop in the first half of plate. Reasons attribute to the less the liquid condensed in the first half of the plate. In addition, since the thermal resistance of liquid film is low, and the condensation rate is high, there is a sudden change in pressure, thus the pressure gradient is larger than that in the second half of the plate.

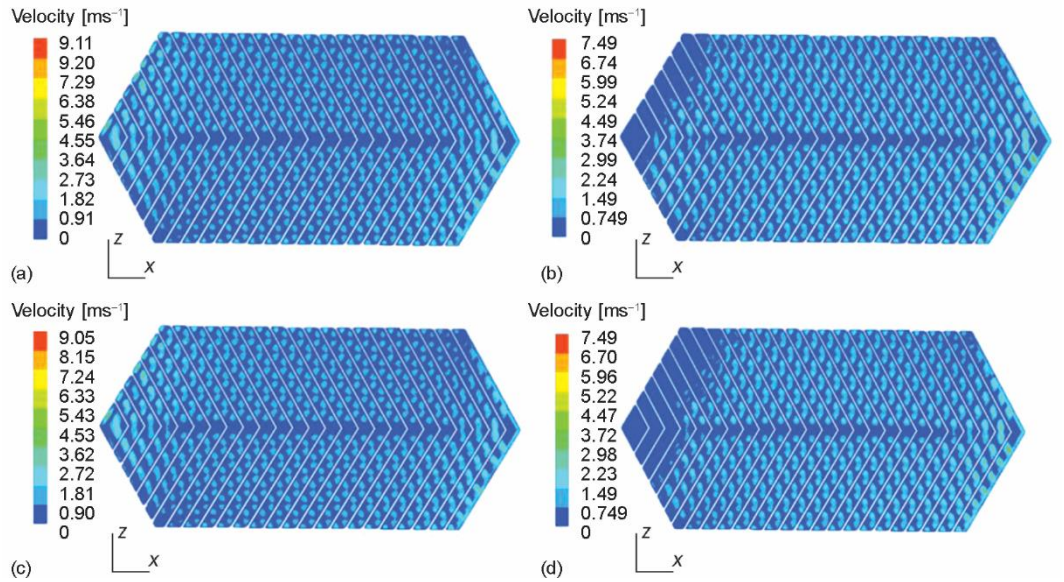

Figure 5. Velocity distribution of PHE; (a) u = 0.5 m/s, Δt = 0 K, vapor phase velocity (b) u = 0.5 m/s, Δt = 0 K, liquid phase velocity, (c) u = 0.5 m/s, Δt = 5 K, vapor phase velocity, (d) u = 0.5 m/s Δt = 5 K, liquid phase velocity

Figures 6(a)-6(d) show that the condensation rate is low at the same position. Reasons attribute to the degree of superheat, which results to the small pressure gradient. These figures show that with the increase of steam flow, the pressure at the inlet and outlet is large, and along the flow direction, the pressure drops fast.

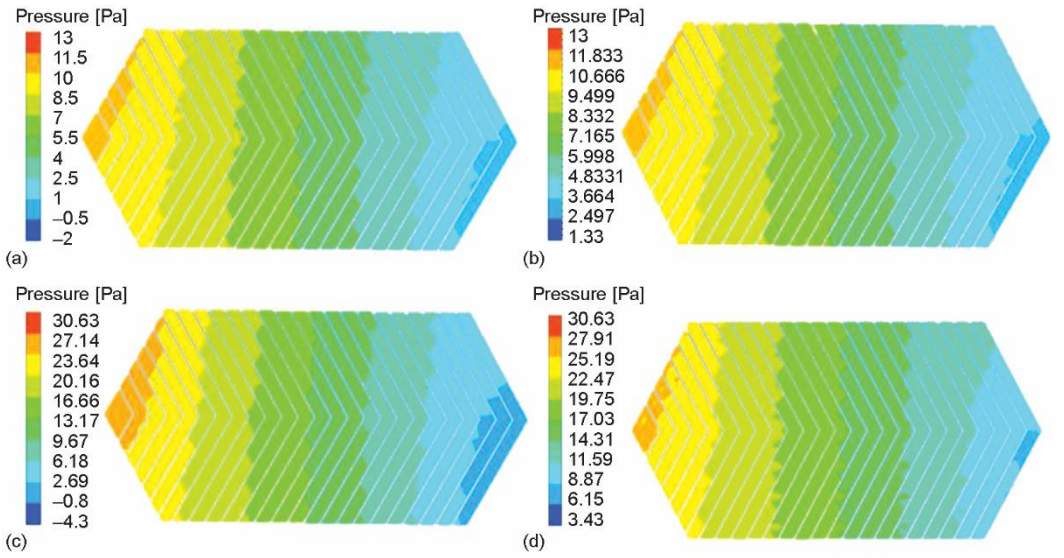

Figure 6. Pressure distribution of PHE; (a) u = 0.5 m/s, Δt = 0 K, (b) u = 0.5 m/s, Δt = 5 K, (c) u = 1 m/s, Δt = 0 K, (d) u = 1 m/s, Δt = 5 K

Temperature distribution characteristics

Figure 7 depicts the temperature distribution of vapor side in a PHE with y = 2 mm cross-section. From fig. 7, we can see that the temperature of vapor becomes lower and lower along the flow direction. When the temperature is lower than the saturation temperature, condensate occurs, releasing latent heat and forming liquid film on the wall. We found that the temperature gradient increases with the increase of velocity and pressure gradient, because the distribution of temperature is strongly influenced by velocity and pressure of vapor. At the same time, considering the fact that liquid film thickness increases with the flow of vapor, due to small temperature different between vapor and plate, its contribution to the condensation rate would be small. Therefore, the temperature gradient of vapor would get smaller and smaller. It is important to point out that the effect of degree of superheat on the condensate process is not negligible.

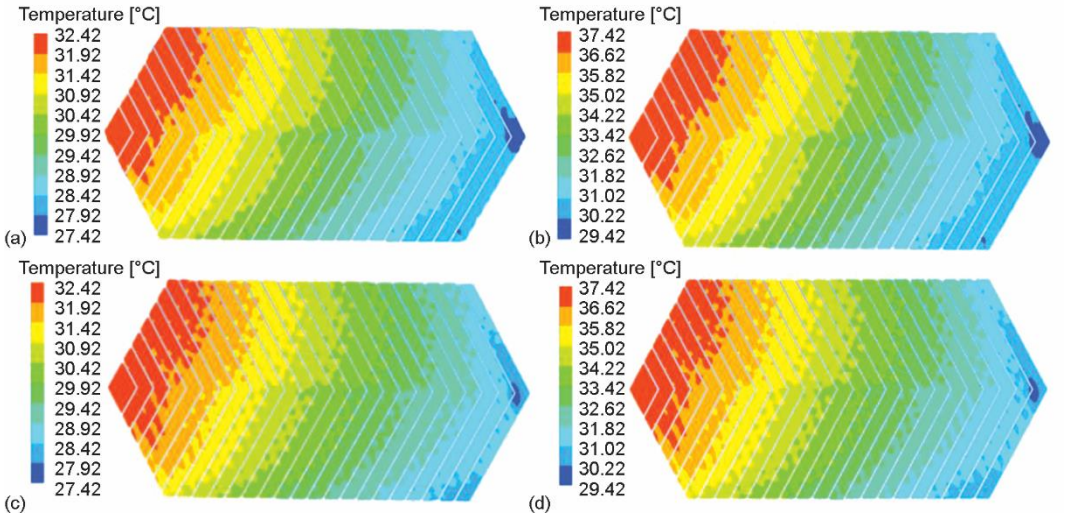

Figure 7. Temperature distribution of PHE; (a) u = 0.5 m/s Δt = 0 K, (b) u = 0.5 m/s Δt = 5 K, (c) u = 1 m/s Δt = 0 K, (d) u = 1 m/s Δt = 5 K

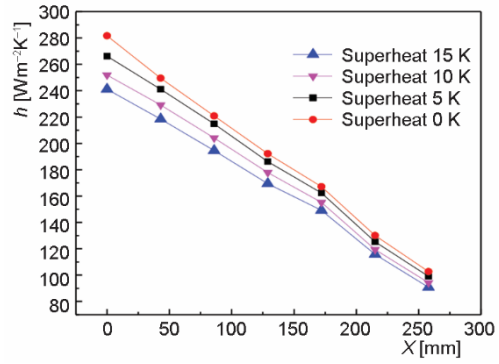

Figure 8. Variation of heat transfer coefficient with degree of superheat

Influence factor

Effect of vapor superheat on condensation heat transfer

Figure 8 displays the condensation heat transfer coefficient for the various degree of superheat. The degree of superheat has a significant influence on the condensation process. With the degree of superheat increase, the condensation heat transfer coefficient decreases at the same position of the plate, which causes the the liquid condensed reducing, as displayed in fig. 8. In addition, the condensation heat transfer coefficient is high due to thin liquid film

and low flow-resistance effects at the entrance. As the condensation process progresses, the condensation heat transfer coefficient begin to decrease.

Effect of mass-flow on condensation heat transfer and pressure drop

Figure 9 displays the condensation heat transfer coefficient for the various mass-flow. It can be found that the condensation heat transfer coefficient increases with the mass-flow increase at the same position of the plate. There are the more liquid condensed and the larger thermal resistance of liquid film due to the increase of mass-flow. However, the latent heat released by vapor condensation is more resulting in the increased the heat transfer coefficient. In addition, under the same mass-flow condition, the condensation heat transfer coefficient decreases with the increase of superheat. Reasons attribute to the degree of superheat, which results to releasing part of latent heat and reducing heat transfer coefficient.

Figure 10 shows the effect of mass-flow on pressure drop. It is found that pressure drop increases with the increase of mass-flow. However, it can be seen that the increase of the degree of superheat leads to a decrease in pressure drop, as shown in fig. 10. The reason is may be attributed to the decrease of condensation rate due to the existence of superheat.

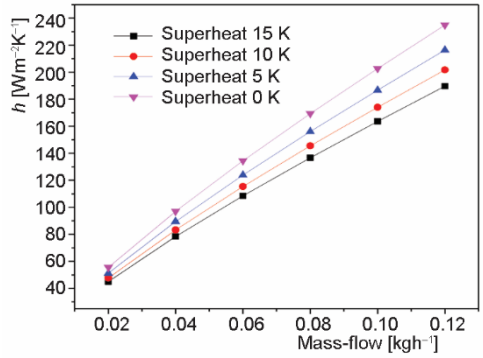

Figure 9. Variation of heat transfer coefficient with mass-flow

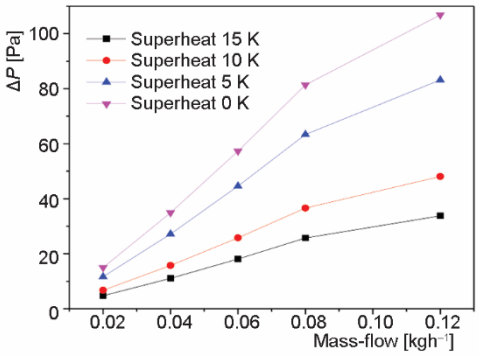

Figure 10. Variation of pressure drop with mass-flow

Effect of drying on condensation heat transfer and pressure drop

Figure 11 displays the condensation heat transfer coefficient for the various dryness. As shown in fig. 11, it can be seen that the condensation heat transfer coefficient increases with the dryness increase under the same mass-flow condition. Furthermore, we can also see that under the same dryness condition, the heat transfer coefficient increases with the increase of mass-flow. Reasons attribute to the decreasing thermal resistance of the liquid film, which is function of the liquid film fluctuate and the shear force of vapor on the liquid film.

Figure 12 displays the pressure drop for the various dryness. It is found that pressure drop also shows an upward trend with the increase of dryness. Furthermore, we can also see that under the same dryness condition, the pressure drop increases with the increase of mass-flow.

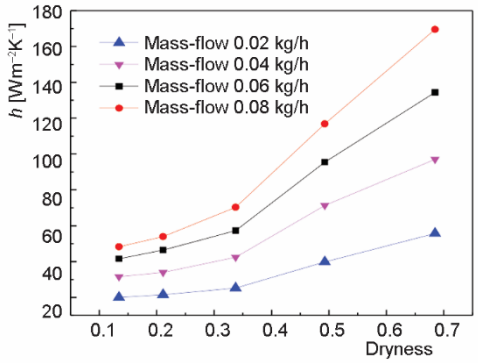

Figure 11. Variation of heat transfer coefficient with dryness

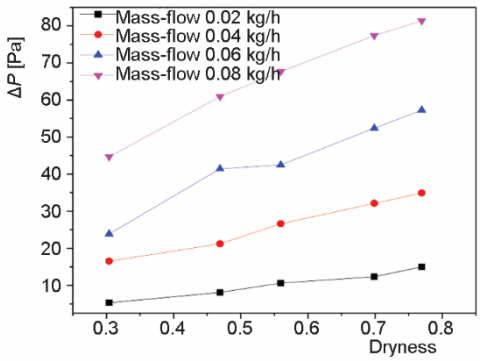

Figure 12. Variation of pressure drop coefficient with dryness

Correlation of heat transfer and resistance criteria

In order to predict the heat transfer coefficients and friction factor for PHE, we tried to derive an empirical correlation. Condensation processes depends on liquid and gas phase operating variables inside PHE. So in the correlations of heat transfer coefficients and friction factor, both liquid and gas phase variables should be considered. All of the effective variables on condensation processes are presented in:

$$h = f[\Delta T, \mathrm{g}(\rho_l - \rho_v), h_{fg}, \sigma, L, \rho_l, c_{p,l}, k_l, \mu_l, u_l] \tag{22}$$

where Δt [K] is the temperature difference between evaporator and condenser, g [ms^{-1}] – the acceleration due to gravity, h_{fg} [Jkg^{-1}] – the latent heat of vaporization, K_l [Wm^{-1}K^{-1}] – the thermal conductivity of fluid, ρ_v [kgm^3] – the density of vapor, $\rho_l - \rho_v$ [kgm^3] – the density difference between liquid and gas, $c_{p,l}$ [Jkg^{-1}] – the specific heat of fluid at constant pressure, μ_l [Pa·s] – the viscosity of the liquid, σ [Nm^{-1}] – the surface tension, u_l [ms^{-1}] – the velocity of condensate liquid, and L [m] – the characteristic size.

Using Buckingham's Pi-theorem, eq. (22) consists of 10 independent variables with four primary dimensions involved, *i. e.*, M [kg], L [m], T [seconds], and t [K]). Therefore, the total numbers of dimensionless parameters that should be included in the analysis is six. The following repeating variables were selected for this analysis to make sure all four major dimensions are involved. The results of dimensional analysis for the specified variables are:

$$\pi_1 = \Delta T^{a_1} L^{b_1} \mu_l^{c_1} c_{p,l}^{d_1} \mathrm{g}(\rho_\mathrm{l} - \rho_\mathrm{v}) \tag{23}$$

$$\pi_2 = \Delta T^{a_2} L^{b_2} \mu_l^{c_2} c_{p,l}^{d_2} h_{fg} \tag{24}$$

$$\pi_3 = \Delta T^{a_3} L^{b_3} \mu_l^{c_3} c_{p,l}^{d_3} \sigma \tag{25}$$

$$\pi_4 = \Delta T^{a_4} L^{b_4} \mu_l^{c_4} c_{p,l}^{d_4} \rho_l \tag{26}$$

$$\pi_5 = \Delta T^{a_5} L^{b_5} \mu_l^{c_5} c_{p,l}^{d_5} k_l \tag{27}$$

$$\pi_6 = \Delta T^{a_6} L^{b_6} \mu_l^{c_6} c_{p,l}^{d_6} u_l \tag{28}$$

By combining the various π terms we get:

– Bond number

$$\frac{\pi_1}{\pi_3} = \frac{\dfrac{\mathrm{g}(\rho_l - \rho_\mathrm{v})L^2}{\sqrt{\Delta T c_{p,l}}\,\mu_l}}{\dfrac{\sigma}{\sqrt{\Delta T c_{p,l}}\,\mu_l}} = \frac{\mathrm{g}(\rho_l - \rho_\mathrm{v})L^2}{\sigma} = \mathrm{Bo} \tag{29}$$

– Jakob number

$$\pi_2 = \frac{h_{fg}}{\Delta T c_{p,l}} = \mathrm{Ja} \tag{30}$$

– Prandtl number

$$\pi_5 = \frac{k_l}{c_{p,l}\mu_l} = \mathrm{Pr} \tag{31}$$

– Reynolds number

$$\pi_4\pi_6 = \frac{\sqrt{\Delta T c_{p,l}}\,\rho_l L}{\mu_l}\frac{u_l}{\sqrt{\Delta T c_{p,l}}} = \frac{\rho_l u_l L}{\mu_l} = \mathrm{Re} \tag{32}$$

Dimensionless correlation for heat transfer coefficients and friction factor of condensation processes is presented in eqs. (33) and (34) based on dimensionless numbers of the process:

$$\mathrm{Nu} = f\left(\mathrm{Re}_l, \mathrm{Pr}_l, \mathrm{Ja}, \mathrm{Bo}\right) \tag{33}$$

$$f = f\left(\mathrm{Re}_l, \mathrm{Re}_\mathrm{v}\right) \tag{34}$$

Eventually, the obtained correlation is:

$$\mathrm{Nu} = a\,\mathrm{Re}_l^b\,\mathrm{Pr}_l^c\,\mathrm{Ja}^d\,\mathrm{Bo}^e \tag{35}$$

$$f = m\,\mathrm{Re}_\mathrm{v}^n\,\mathrm{Re}_l^r \tag{36}$$

The coefficient *a*-*r* are determined from the simulation data using non-linear curve fitting technique. Where $a = 0.017$, $b = 0.795$, $c = -0.268$, $d = -1.64$, $e = 0.014$, $m = 1.059$, $n = 0.561$, $r = -1.342$. Therefore, Nu and *f* are expressed by:

$$\mathrm{Nu} = 0.017\,\mathrm{Re}_l^{0.795}\,\mathrm{Pr}_l^{-0.268}\,\mathrm{Ja}^{-1.64}\,\mathrm{Bo}^{0.014} \quad 100 < \mathrm{Re}_l < 1000 \tag{37}$$

$$f = 1.059\,\mathrm{Re}_\mathrm{v}^{0.561}\,\mathrm{Re}_l^{-1.342} \quad 100 < \mathrm{Re}_l < 1000 \tag{38}$$

The predicted Nu and *f* by correlations (37) and (38) are compared with experimental data [22] in tab. 2. As it can be seen, compare experimental data with predicting data of heat transfer coefficients and friction factor, their relatively error are less than 5%. Meanwhile, the value of regression coefficient, R^2, for this correlation is 0.999. In addition, residual analysis is performed to increase the accuracy of the prediction. The residual analysis shows that the distribution of standardized residuals is normal. The results show that the presented correlations can predict heat transfer coefficients and friction factor of condensation processes with high accuracy in different operational conditions.

Table 2. Predicted data *vs.* experimental data

Operational conditions	Experimental data, Nu	Predict data, Nu	Relative error	Standardized residual	Experimental data, *f*	Predict data, *f*	Relative error	Standardized residual
1	11.055	11.101	0.42%	–0.549539492	69.402	70.594	1.72%	–1.05153754
2	19.274	19.320	0.24%	–0.549539492	40.417	41.106	1.70%	-0.60780987
3	26.698	26.753	0.21%	–0.657058088	29.459	29.958	1.69%	–0.44019902
4	33.66	33.740	0.24%	–0.955720855	23.538	23.935	1.69%	–0.350218459
5	40.27	40.357	0.22%	–1.03934643	19.778	20.111	1.68%	–0.293760068
6	10.186	10.158	–0.27%	0.334502299	63.491	60.832	–4.19%	2.34566973
7	17.757	17.675	–0.46%	0.979613877	36.975	35.421	–4.20%	1.370880316
8	24.595	24.472	–0.50%	1.469420815	26.95	25.815	–4.21%	1.001254285
9	31.005	30.860	–0.47%	1.73224405	21.533	20.625	–4.22%	0.801003428
10	37.069	36.916	–0.49%	1.827816136	18.093	17.33	–4.22%	0.673089885
11	9.495	9.507	0.13%	–0.143358128	51.957	53.071	2.14%	–0.982728875
12	16.552	16.541	–0.06%	0.131411618	30.258	30.902	2.13%	–0.568112563
13	22.924	22.899	–0.11%	0.298662767	22.054	22.522	2.12%	–0.412851987
14	28.898	28.872	–0.09%	0.310609278	17.621	17.994	2.12%	–0.329046562
15	34.576	34.541	–0.10%	0.418127874	14.806	15.119	2.11%	–0.27611682

Conclusions

In this paper, a numerical model was established to investigate the condensation heat transfer and pressure drop characteristics for PHE. It discussed the influence of the degree of superheat, mass-flow and dryness on pressure drop and heat transfer coefficient. Additionally, we attempted to propose a new correlation of the condensation heat transfer and pressure drop, for PHE. The conclusions are as follows.

- The pressure drop and heat transfer coefficient both increase with the increase of dryness, degree of superheat and mass-flow, and the various positions of the plate have little effect on them, this is due to the existence of heat and mass transfer resistance in PHE.
- The correlation for estimating the heat transfer and pressure drop during the condensation process of PHE, could be applied to the cold end system of thermal power unit.

Acknowledgment

This work was supported by the National Key R&D Program of China (No. 2017YFB0902100).

Reference

[1] Wang, L., *et al.*, *Plate Heat Exchangers e Design, Applications and Performance*, WIT Press, Southampton, UK, 2007
[2] Thome, J. R., *et al.*, Two-Phase Heat Transfer and Pressure Drop Within Plate Heat Exchangers, *Encycl. Two-Phase Heat Transf.,* Flow II (2015), Oct., pp. 145-215

[3] Sarraf, K., *et al.*, Complex 3D-Flow Analysis and corruGation Angle Effect in Plate Heat Exchangers, *Int. J. Therm. Sci., 94* (2015), Aug., pp. 126-138
[4] Lee, J., Lee, K. S., Flow Characteristics and Thermal Performance in Chevron Type Plate Heat Exchangers, *Int. J. Heat Mass Transf., 78* (2014), Nov., pp. 699-706
[5] Gherasim, I., *et al.,* Heat Transfer and Fluid-flow in a Plate Heat Exchanger Part II: Assessment of Laminar and Two-Equation Turbulent Models, *Int. J. Therm. Sci., 50* (2011), 8, pp. 1499-1511
[6] López-Belchí, A., Illán-Gómez, F., Evaluation of a Condenser Based on Mini-Channels Technology Working with R410A and R32. Experimental Data and Performance Estimate, *Appl. Energy, 202* (2017), Sept., pp. 112-124
[7] Abadi, S. M. A. N. R., *et al.,* Numerical Simulation of Condensation Inside Inclined Smooth Tube, *Chem. Eng. Sci., 182* (2018), June, pp. 132-145
[8] Abadi, S. M. A. N. R., *et al.,* Numerical Investigation of Condensation Inside an Inclined Smooth Tube, in: *Proceedings*, 13th Int. Conf. Heat Transfer, Fluid Mechanics and Thermodynamics, Portoroz, Slovenia, 2017, pp. pp. 572-576
[9] Longo, G.A., *et al.,* Condensation of the Low GWP Refrigerant HFO1234ze (E) Inside a Brazed Plate Heat Exchanger, *Int. J. Refrig., 38* (2014), Feb., pp. 250-259
[10] Jokar, A., *et al.,* Dimensional Analysis on the Evaporation and Condensation of Refrigerant R-134a in Mini-channel Plate Heat Exchanger, *Appl. Therm. Eng., 26* (2006), 17-18, pp. 2287-2300
[11] Wang, L. K., *et al.,* Pressure Drop Analysis of Steam Condensation in a Plate Heat exchanger, *Heat Transfer Eng., 20* (1999), 1, pp. 71-77
[12] Han, X. H., *et al.,* A Numerical and Experimental Study of Chevron, Corrugated-Plate Heat Exchangers, *Int. Commun. Heat Mass. Transf., 37* (2010), 8, pp. 1008-1014
[13] Shi, Z. Y., *et al*., Experimental Investigation on Condensation Heat Transfer and Pressure Drop of R134a in a Plate Heat Exchanger, *Heat Mass. Tran., 46* (2010), 10, pp. 1177-1185
[14] Nusselt, W., The Condensation of Steam on Cooled Surfaces, *Z Des Vereines Dtsch Ingenieure, 60* (1916), pp. 541-575
[15] Bromley, L., Effect of Heat Capacity of Condensate, *Ind. Eng. Chem., 44* (1952), 12, pp. 2966-2969
[16] Jokar, A., *et al.,* Condensation Heat Transfer and Pressure Drop of Brazed Plate Heat Exchangers Using Refrigerant R134a, *J. Enhanced Heat Transfer, 11* (2004), 2, pp. 161-182
[17] Kuo, W. S., *et al*., Condensation Heat Transfer and Pressure Drop of Refrigerant R410A Flow in a Vertical Plate Heat Exchanger, *Int. J. Heat Mass. Transfer, 48* (2005), 25-26, pp. 5205-5220
[18] Hirt, C. W., Nichols, B. D., Volume of Fluid (VOF) Method for the Dynamics of Free Boundaries, *J. Comput. Phys., 39* (1981), 1, pp. 201-225
[19] Brackbill, J., *et al.,* A Continuum Method for Modeling Surface Tension, *J. Comput. Phys., 100* (1992), 2, pp. 335-54
[20] Lee, W. H., *A Pressure Iteration Scheme for Two-Phase Flow Modeling,* Hemisphere, Washington DC, 1980
[21] Alexiades, V., Solomon, A. D., *Mathematical Modeling of Melting and Freezing Processes*, Hemisphere Publishing, Washington DC, USA, 1993
[22] Wang, Z., *et al.,* Flowing Condensation Heat Transfer Law of Steam in Complex Channels, *Journal of Engineering Thermophysics 16* (1995), 1, pp. 70-74

Paper submitted: September 14, 2019
Paper revised: February 3, 2020
Paper accepted: March 10, 2020